Optimization of Contact Cathode Composition Based on La0.8Sr0.2MnO3±δ for SOFC Stacks

ECS Transactions, 103 (1) 1453-1460 (2021)
10.1149/10301.1453ecst ©The Electrochemical Society

Optimization of Contact Cathode Composition based on $La_{0.8}Sr_{0.2}MnO_{3\pm\delta}$ for SOFC Stacks

D. V. Matveev, Yu. S. Fedotov, A. I. Ivanov, E. A. Agarkova, S. I. Bredikhin, V. V. Kharton

Osipyan Institute of Solid State Physics RAS, Chernogolovka, Moscow region 142432, Russia

The formation of stable contact layers with minimum electrical resistivity at the electrode/interconnector interface is an important task for planar SOFC stack fabrication. This work was centered on the search for optimum processing conditions of the $La_{0.8}Sr_{0.2}MnO_{3\pm\delta}$ (LSM) based contact pastes without inorganic additives. The ball-milling conditions and contact paste composition were optimized taking into account the LSM particle size, sintering, a possibility of partial phase decomposition, and electrical conductivity of the resultant cathode contacts. Testing of the model SOFC stack with Crofer 22H interconnectors revealed sufficient adhesion, porosity, conductivity and stability of porous LSM contact layers.

Introduction

Power generation systems based on planar solid oxide fuel cells (SOFCs) have numerous stationary and mobile applications due to their high efficiency, fuel flexibility, a possibility to recover exhaust heat and other advantages. The key unit of such systems is a stack which comprises, in particular, multilayered ceramic fuel cell plates and stainless-steel interconnectors placed between them (1-3). One example of the planar SOFC and stack architecture, tested in this work, is presented in Fig.1. Reliable adhesion and current collection at the interface between the metallic current collectors and SOFC electrodes are necessary to suppress any power losses due to contact resistance (4,5). At the anode side of ceramic SOFC plates, high quality contacts can be obtained using metal (e.g., nickel) meshes. In the cathode chamber, however, these meshes would be quickly oxidized in flowing air at elevated temperatures. Therefore, in order to form reliable contacts between the SOFC cathode and current collector, electron-conducting contact pastes based on oxide ceramics or glass-ceramics should be used (6-8).

The research group at the Osipyan Institute of Solid State Physics RAS conducts systematic R&D in the field of SOFC-based systems, including processing and characterization of novel materials and SOFC components (9-12), fabrication of the membrane-electrode assemblies (MEAs) (2, 13), and testing and optimization of the planar SOFC stacks and power generators. An important task in this direction is to ensure stable electrical and mechanical contacts between the steel current collector with oxide protective coating and SOFC cathode, enabling at least 10,000 h operation (14, 15). In the present work, pastes made of lanthanum-strontium manganite (LSM) were chosen as the cathode contact composition providing mechanical and chemical

compatibility with other components of the stack (16). In particular, effects of ball-milling on the morphology of the LSM powder and transport properties of the LSM contact layers under SOFC stack operating conditions were assessed.

Experimental

Synthesis and characterization

The synthesis of single-phase powders of perovskite-type $La_{0.8}Sr_{0.2}MnO_{3\pm\delta}$ (LSM) was carried out by the glycine-nitrate method (17) using high-purity $La(NO_3)_3$ $6H_2O$, $Sr(NO_3)_2$ and $Mn(CH_3COO)_2$ $4H_2O$ as starting materials. The stoichiometric amounts of metal salts were dissolved in distilled water with subsequent addition of glycine. The resulting mixture was intensively stirred under moderate heating; upon evaporation and subsequent ignition of the mixture, a fine powder was obtained. The reaction product was calcined at 700 °C with isothermal holding for 5 hours in air in order to remove carbon-containing residues and to form single perovskite-type phase. The pre-final annealing was carried out at 750 °C.

Phase composition and structure of the powders were studied by X-ray diffraction (XRD) employing a Siemens D-500 instrument with CuK_α radiation. Characterization of the powder morphology was carried out by the transmission electron microscopy (JEOL JEM-100CX). Microstructure of the materials prior to and after fuel cell operation was analyzed on a Supra 50 VP scanning electron microscope.

Paste fabrication and conductivity tests

As-prepared LSM powder was milled in the planetary-type mill Pulverisette 6 (Fritsch) for 500 min at a speed varying from 200 to 600 rpm. Milling was carried out in ethanol using zirconia balls (diameter of 5 mm). Then this LSM powder was in consecutive order dried and mixed with 9 wt.% polyvinyl butyral (PVB, Mowital B75H) as binder, 2 wt.% diethyl adipate as plasticizer, 2 wt.% diamine RRT as dispersant and a mixture of toluene and butanol (70:30 vol.%) as solvent. The slurry was homogenized in a Thinky ARE-250 planetary mixer.

For the contact material conductivity tests, platinum electrodes were deposited onto one side of yttria-stabilized zirconia (YSZ) solid electrolyte ceramics (∅ 21 mm) produced by NEVZ-Ceramics (10). The LSM strips (width of 4-5 mm) were screen-printed (Mat S45, Ekra, Germany) onto the surface of YSZ electrolyte with Pt electrodes and dried for 1 hour at 100 °C. Loading of the LSM strips was similar to that used for SOFC assembling. Finally, platinum wires were attached to the free surfaces of the Pt electrodes. The electrical resistance measurements were carried out in the temperature range 600-950 °C on heating and subsequent cooling in air using a Gamry Reference 3000 potentiostat/galvanostat/ZRA.

Fuel cell stacking and testing

For testing of the cathode contact materials under SOFC operating conditions, a model stack comprising two commercial MEAs NextCell-10 supplied by FuelCellMaterials, USA (Fig. 1(a)). For these MEAs, the geometric area of each electrode was 81 cm^2. The MEAs were sandwitched between three stainless-steel

current collectors made of Crofer 22H (ThyssenKrupp) with electrodeposited protective layers of metallic Ni (14,15), Fig.2(b). The stack geometry is illustrated by Figure 1(c). The main steps of the stack assembling procedure included:
(i) LSM paste layer was applied onto the cathode side of the metal current collectors;
(ii) MEAs were placed onto these collectors with subsequent deposition of glass-ceramic sealant (Kerafol ST K02);
(iii) Ni meshes were placed onto the MEA anodes; then the anode contact slurry was deposited onto these meshes;
(iv) Following final assembling of the bipolar plates into stack, mechanical load of 0.4 kg/cm^2 was applied.

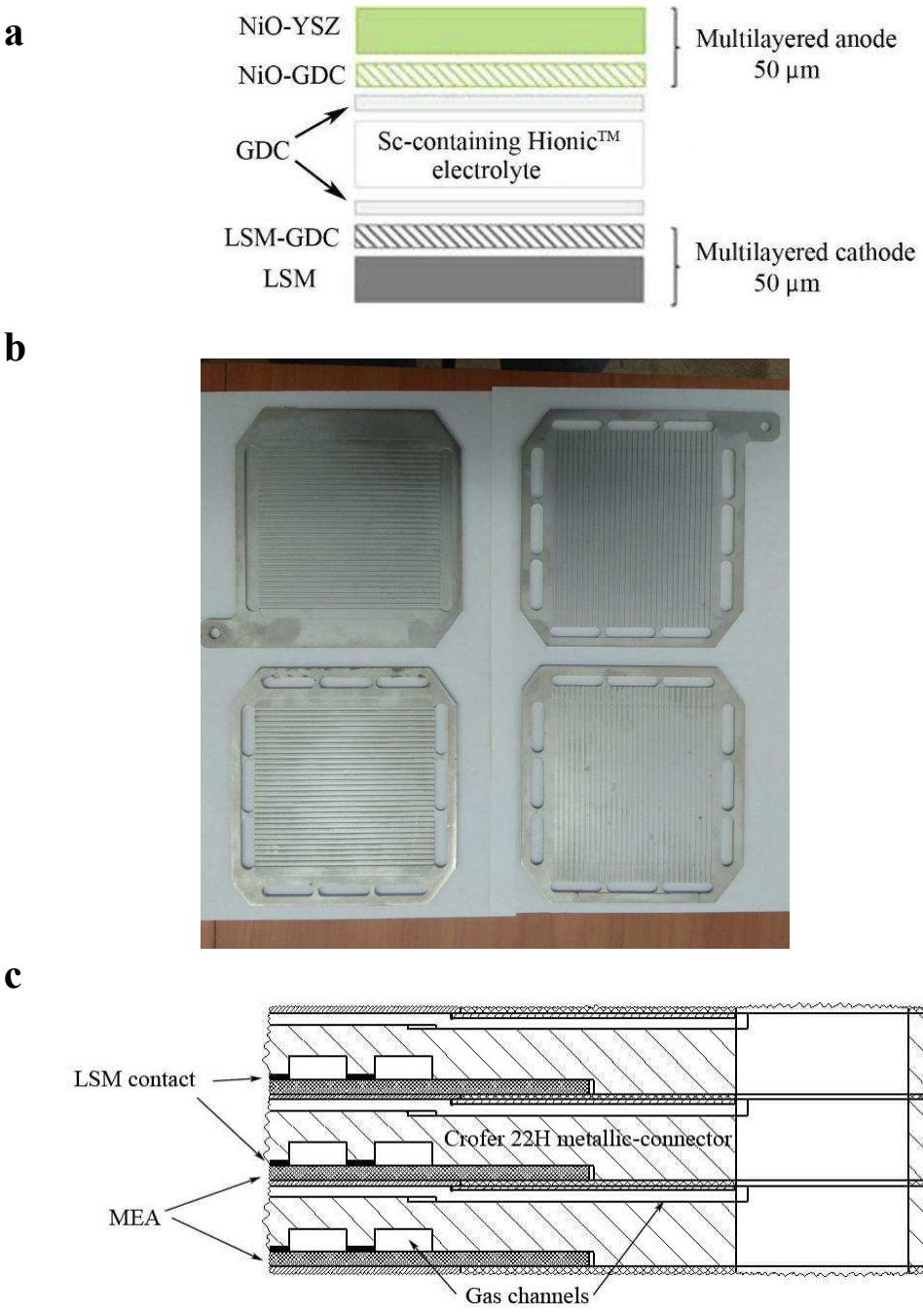

Figure 1. Architecture of the MEA used for stack assembling (a), photograph of the stainles steel current collectors with protective Ni layers (b), and schematic drawing of the stack cross-section (c).

Pressurization and sealing of the model SOFC stack were carried out in a shell-type furnace. The temperature vs. time profile used for sealing is shown in Figure 2. The mechanical load applied to the stack during sealing was 0.4 kg/cm^2. The measurements of the current-voltage (I-V) dependencies and impedance spectra of the assembly were performed employing a Reference 3000 potentiostat-galvanostat (Gamry, USA) equipped with an additional Reference 30K Booster module. These tests were carried out at 845 °C, using pure hydrogen as fuel and atmospheric air as oxidant.

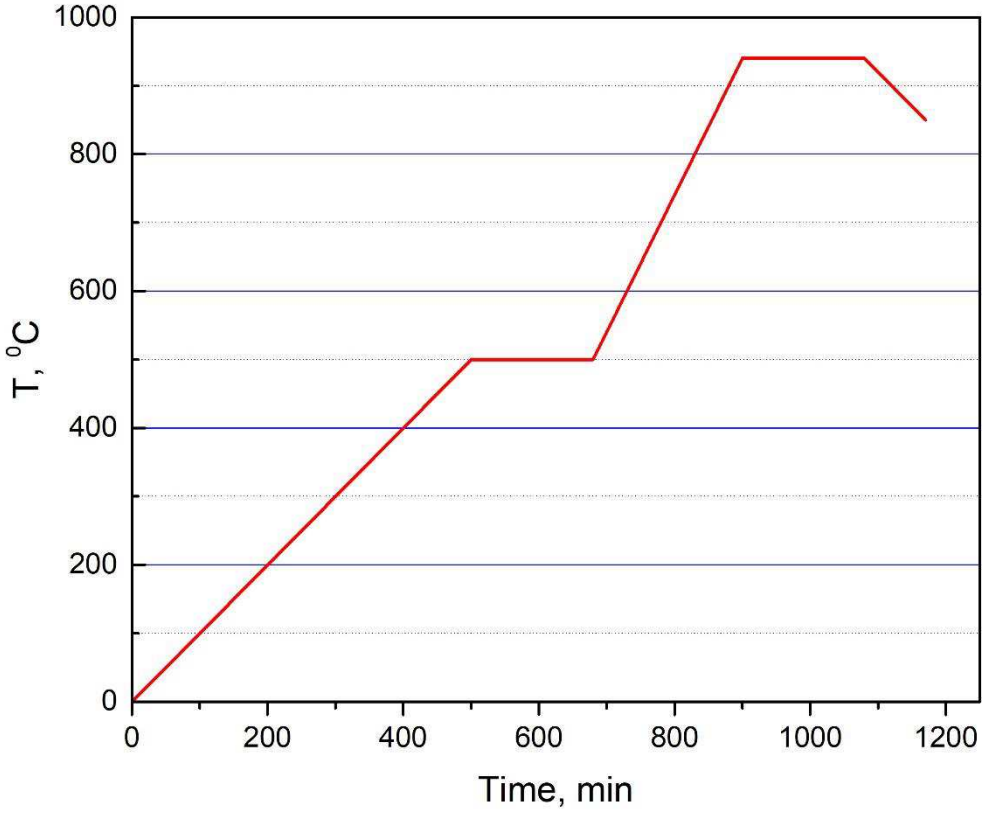

Figure 2. Temperature profile used for the SOFC stack sealing.

Results and discussion

Examples of the XRD patterns of as-prepared and ball-milled LSM powders are presented in Figure 3. The as-synthesized LSM, and the powders milled under mild conditions (e.g., 200 rpm and 500 min), are single-phase. However, grinding of the initially single-phase powder during 500 min at 300 rpm results in an appearance of additional XRD reflections corresponding to $Sr(OH)_2$ and $MnCO_3$ phases. Further increase in the milling speed leads to increasing amount of the impurity phases. The latter factor is responsible for worsening of the contact adhesion at sintering temperatures lower than 950 °C. At the same time, ball-milling at 200 rpm is sufficient to decrease the size of LSM particle agglomerates down to the submicron level (Fig.4).

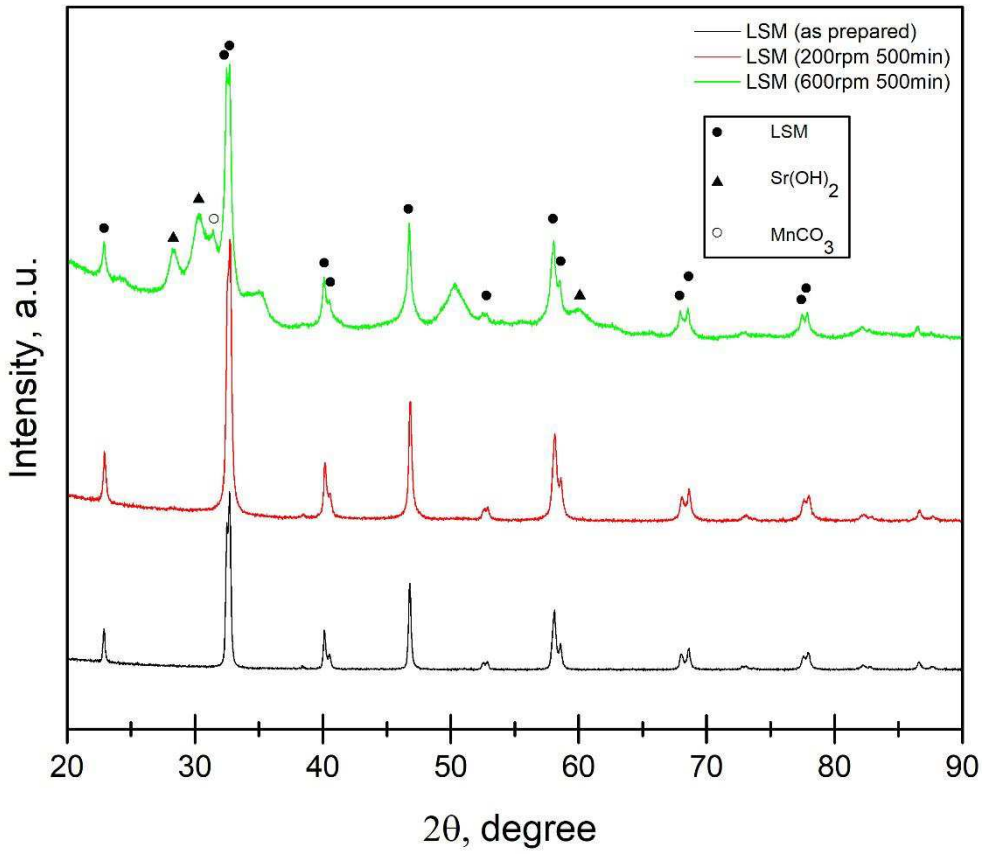

Figure 3. Examples of the XRD patterns of as-prepared and ball-milled LSM powders.

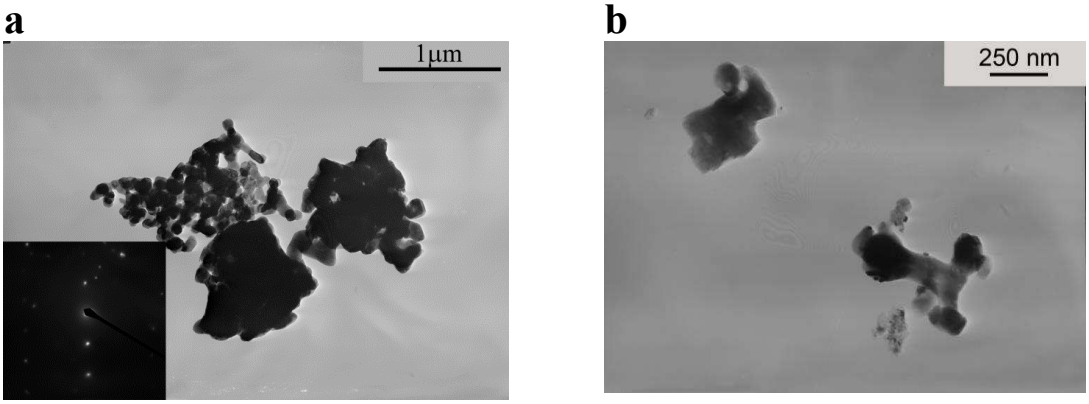

Figure 4. Comparison of the TEM images of as-prepared LSM powder (a) and the powder milled at 200 rpm for 500 min (b).

The results of the contact resistivity measurements illustrated in Figure 5 confirm that the contact layers, based on the stoichiometric lanthanum-strontium manganite powder pre-activated by grinding at a speed of 200 rpm, exhibit optimum properties. At the SOFC operation temperature, the specific electrical resistivity of pre-grinded LSM after sintering is three times lower than the resistance of as prepared and sintered LSM: $0.7 \cdot 10^{-3}$ Ω·m vs. $2.2 \cdot 10^{-3}$ mΩ·m, respectively. When the ball-milling time and/or speed increase and perovskite phase decomposition starts, the contact resistance increases.

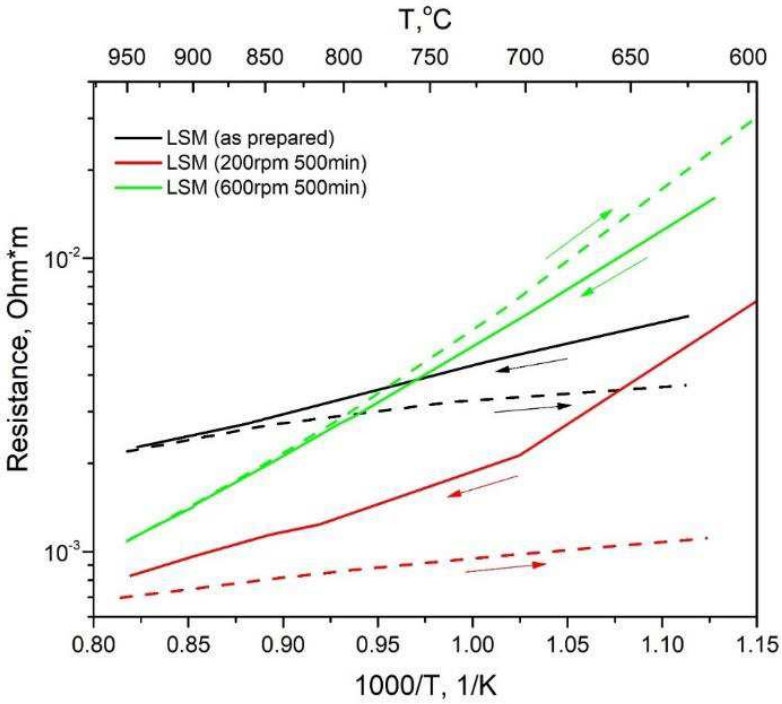

Figure 5. Temperature dependences of the specific electrical resistivity of the LSM contact layers fabricated using as-prepared and ball-milled powders. The arrows indicate heating (solid lines) and cooling (dashed lines).

Typical microstructures of the cathode with LSM contact layer (a) and anode (b) after the stack operation during approximately 100 hours are shown in Figure 6. It can be clearly observed, in particular, that the conducting contact layer has a good adhesion to the MEA electrode. Its high porosity is advantageous for the gas diffusion, necessary to avoid a significant contraction of the active electrode area under the contact with current collector.

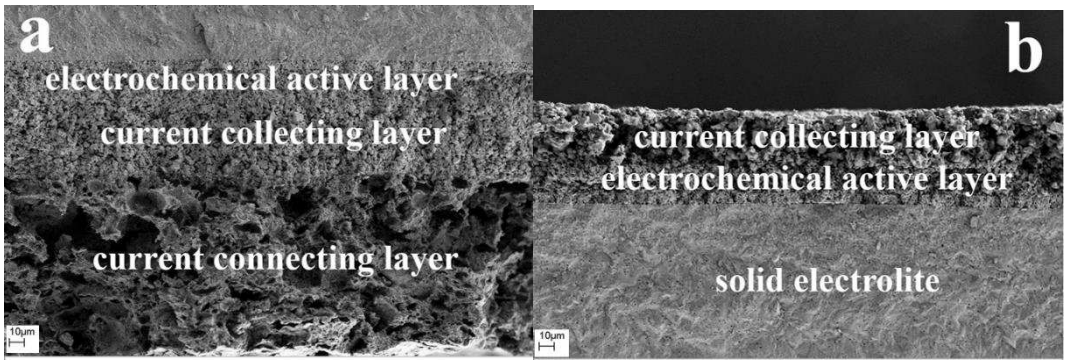

Figure 6. SEM-images of the SOFC cross-sections with contact layers: (a) cathode side, (b) anode side.

Following sealing of the SOFC stack accompanied with sintering of the contact layers, the electrochemical tests were carried out. Pure hydrogen (flow rate of 200 ml/min) was supplied as a fuel; atmospheric air (approx.. 500 ml/min) acted as an oxidant. After the anode reduction, the open circuit voltage (OCV) reached 1.08 V for each of the MEAs. In order to achieve a steady-state regime and to check stability of the contacts, the stack was initially tested under a current load of 5 A for 10 hours.

Figure 7 shows the voltage vs. time dependence for one of the MEAs in these conditions. The stationary regime with a voltage of about 0.96 V was achieved during approximately 7 hours after the test start. Further investigations revealed no significant degradation in the stack performance.

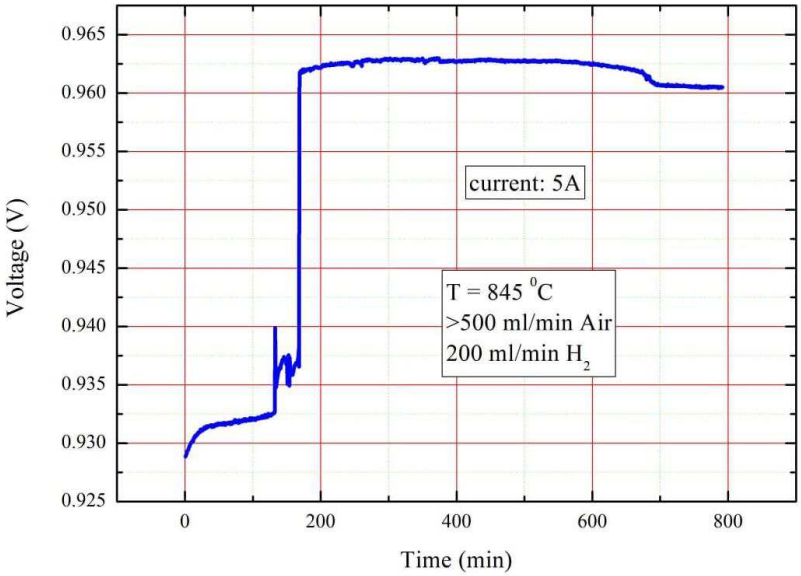

Figure 7. Time dependence of the voltage per one MEA during the electrode activation under 5 A current load.

Conclusions

The formation of stable contact layers with minimum electrical resistivity at the electrode/interconnector interfaces is an important task for planar SOFC stack fabrication. This work was focused on the optimization of processing conditions of the $La_{0.8}Sr_{0.2}MnO_{3\pm\delta}$ (LSM) based contact pastes without other inorganic additives. The ball-milling conditions and contact paste composition were optimized accounting for the LSM particle size, powder morphology, sintering and electrical resistance of the resultant cathode contacts. Although increasing ball-milling time and/or speed makes it possible to decrease particle size in the glycine-nitrate synthesized powders, it leads also to the partial decomposition of perovskite-type LSM phase, which is associated with worse sintering and lower conductivity. An optimum combination of the functional properties was achieved for mild conditions, namely the rotation speed and milling time values close to 200 rpm and 500 min, respectively. Testing of the model SOFC stack with surface-protected Crofer 22H interconnectors confirmed sufficient adhesion, porosity and conductivity of the porous LSM contact layers. No traces of degradation and materials interaction were revealed.

Acknowledgments

This work was financially supported by the Russian Science Foundation project 17-79-30071 “Scientifically grounded optimization of power and mass-dimensional characteristics of planar SOFC stacks and development of fuel processor for highly efficient transport and stationary power plants”.

References

1. P. Holtappels U. Stimming, *Handbook of Fuel Cells, 2010.*
2. I.N. Burmistrov, D.A. Agarkov, E.V. Korovkin, D.V. Yalovenko, S.I. Bredikhin, *Russ. J. Electrochem.,* **53** (8), 873, 2017.
3. T.-L Wen, D. Wang, M Chen, H Tu, Z Lu, Z Zhang, H Nie, W Huang, *Solid State Ionics,* **148** (3-4), 513, 2002.
4. P. Holtappels, C. Bagger, *J. Europ. Ceram. Soc.,* **22** (1), 41, 2002.
5. K.D. Seo, Y.J. Kim, J.-Y Park, H.-T. Lim, *Int. J. Hydrogen Energy,* **43** (4), 2349, 2018.
6. Z. Yang, G. Xia, P. Singh, J.W. Stevenson, *J. Power Sources*, **155**, 246, 2006.
7. W.B. Guan, H.J. Zhai, L. Jin, T.S. Li, W.G. Wang, *Fuel Cells*, **11** (3), 445, 2011.
8. M.C. Tucker, L.C. DeJonghe, V. Garcia-Negron, R. Trejo, E. Lara-Curzio, *J. Power Sources*, **239**, 315, 2013.
9. E.A. Agarkova, I.N. Burmistrov, D.A. Agarkov, O.Yu. Zadorozhnaya, A.V. Shipilova, A.A. Solovyev, Yu.K. Nepochatov, S.I. Bredikhin, *Mater. Lett.,* **283**, 128752, 2021.
10. E.A. Agarkova, D.A. Agarkov, I.N. Burmistrov, O.Yu. Zadorozhnaya, D.V. Yalovenko, Yu.K. Nepochatov, S.I. Bredikhin, *Russ. J. Electrochem.,* **56** (2), 132, 2020.
11. O.Yu. Zadorozhnaya, E.A. Agarkova, O.V. Tiunova, Yu.K. Nepochatov, *Russ. J. Electrochem.,* **56** (2), 124, 2020.
12. E.V. Tsipis, I.N. Burmistrov, D.A. Agarkov, D.V. Matveev, V.V. Kharton, S.I. Bredikhin, *Nanotechnologies in Russia,* **15** (3-6), 356, 2020.
13. I.N. Burmistrov, D.A. Agarkov, F.M. Tsybrov, S.I. Bredikhin, Russ. J. Electrochem., 52 (7), 669, 2016.
14. N.V. Demeneva, O.V. Kononenko, D.V. Matveev, V.V. Kharton, S.I. Bredihin, *Mater. Lett.,* **240**, 201, 2019.
15. N.V. Demeneva, D.V. Matveev, V.V. Kharton, S.I. Bredikhin, *Russ. J. Electrochem.,* **52** (7), 678, 2016.
16. X. Luo, Y. Yang, Y. Yang, D. Tian, X. Lu, Y. Chen, Q. Huang, B. Lin, *Electrochim. Acta,* **260**, 121, 2018.
17. A.P. Jamale, A. Natoli, L.D. Jadhav, *J. Phys. Chem. Solids,* **148**, 109723, 2021.